Determining the electrochemical transport parameters of sodium-ions in hard carbon composite electrodes

D. Ledwoch [a], L. Komsiyska [c], E-M. Hammer [b], K. Smith [b], P. R. Shearing [a,e], D. J. L. Brett [a,e*] and E. Kendrick [a,d,e*],

[a] Electrochemical Innovation Lab, Department of Chemical Engineering, University College London, London WC1E 6BT; United Kingdom

[b] Johnson Matthey Technology Centre, Reading RG4 9NH; United Kingdom

[c] Technische Hochschule Ingolstadt, Institute for Innovative Mobility, Ingolstadt, Germany

[d] School of Metallurgy and Materials, University of Birmingham, Edgbaston, Birmingham, B15 2TT, United Kingdom

[e] The Faraday Institution, Quad One, Harwell Science and Innovation Campus, Didcot, United Kingdom

[*]Corresponding Author's E-mail Address: e.kendrick@bham.ac.uk, and d.brett@ucl.ac.uk

Abstract

Sodium-ion batteries offer advantages over conventional Li-ion batteries, including cost and safety. However, much less is known about their operation and performance properties, particularly at the anode. The electron and ion transport in the active materials and composite electrode significantly impact battery performance. Understanding the changes in transport properties as a function of state-of-charge and state-of-health is essential for effective electrode design and performance assessment. In this work, the resistivity and diffusivity of sodium transport in hard carbon composite electrodes are studied at different states-of-health, using Galvanostatic Intermittent Titration Technique (GITT), Electrochemical Impedance Spectroscopy (EIS), and Electrochemical Potential Spectroscopy (EPS) in a stable 3-electrode test cell configuration. The reference electrode eliminated some voltage errors arising from the overpotentials on the counter electrode. The resistance contributions from the surface electrolyte interface, electrolyte transport in the electrode pores, and the charge transfer

resistance are extrapolated from the impedance measurements and the diffusion coefficient from the GITT and EPS. The different techniques indicate similar trends in the diffusion coefficient during sodiation, desodiation, and ageing, although different orders of magnitude were observed between the EPS and GITT data. The accuracy of the parameters calculated using the different electrochemical techniques is discussed in detail.

Keywords (5): Batteries; Hard carbon; Diffusion; Electrochemical Impedance Spectroscopy; Galvanostatic Intermittent Titration Technique; Electrochemical Potential Spectroscopy.

1. Introduction

The commercialization of the lithium-ion battery (LIB) in 1991 revolutionized the portable electronics market and is the preferred battery technology for hybrid and fully electric vehicles.[1–3] Although vehicle propulsion is currently almost exclusively dominated by LIB's, other technologies have potential advantages, such as sodium-ion batteries (NIB's), which offer lower cost and improved safety.[4] However, there are challenges in delivering the high power required for many of these applications, and improvements in understanding the transport limitations are required.[5] Hard carbon (HC) is typically used as the negative electrode, combined with organic carbonate-based electrolytes, and exhibits reversible capacities of 250 to 330 mAh g^{-1} with good cycle-life stability.[6–9] HC is described as a non-graphitic carbon with a larger d-spacing than graphite. The mixed sp^2 and sp^3 hybridization cause a cross-linking between the layers, which induces a lack of long-range ordering in the c-direction, but enhances the electronic conductivity in the a and b directions.[10] Studies on the intercalation mechanism of sodium-ions into HC and graphite-like materials have been published; however, the process is still not fully understood.[11–20]

Understanding the electronic and ionic transport limitations at the positive and negative electrode and within the electrolyte is required to design higher power, longer life and higher capacity electrodes.[5] These parameters can be used in multi-scale models to predict performance properties and battery state of health. including an understanding of the ion diffusion and reaction mechanisms at the anode, regardless of the charge carrying ion, effective

materials selection, and electrode design.[21] Although density-functional theory (DFT) calculations and numerous experiments show similar mobility of sodium-ions within electrolytes and electrodes compared to lithium-ions, their larger ion radius induces greater mechanical stress in the active materials during sodiation.[22–26] Different processes occur, depending on the type of active material; intercalation, alloying, stripping and plating metals. In all cases, the diffusion of carrier ions is important to consider, both within the electrolyte but also within the active material. The rate of electrochemical reactions depends on material characteristics. However, the reaction rates and overpotentials are also influenced by the electrode composition itself. Investigating ion diffusion as a function of state-of-charge (SoC) and state-of-health (SoH) is essential for effective electrode design and performance assessment.[6,27] A full understanding of SoC related diffusion coefficients can help to optimise the charge and discharge procedures further and stabilize reaction processes. Several different electrochemical techniques can be utilized to study these processes; GITT, EPS and EIS are all commonly used in battery research to investigate the properties of cathode and anode materials and calculate diffusion coefficients.[6,12,18,19,28–33] It has been shown previously that the electrode composition impacts the observed electrochemical properties extracted using GITT and EIS techniques.[34,35]

2. Electrochemical Test Methods

The parameters in the test set-up affect the accuracy of constant current, voltage and EIS measurements, and in addition, many more assumptions are made to extract the kinetics and thermodynamics information from these techniques. Often differences between the experimental set-up and the reported assumptions make a comparison between reported values difficult. For example, the initial intermittent titration methods GITT [30] and PITT [36] were derived for diffusion in a thin film rather than a porous electrode, and therefore the electrode area used in the diffusion coefficient calculations was related to the thin film area. Too short relaxation times between pulses means that open circuit voltage (OCV) is not reached, leading to errors, particularly if using the voltages at the beginning and end of the GITT pulse. Greater

accuracy can be obtained if the current or voltage pulse tail is used for parameter extraction, which provides a greater number of data points for fitting. In this respect, the Sand or Cotrell equations for current (GITT) or voltage (PITT) pulses, respectively.[21] The original assumptions of thin-film electrodes have been modified for porous electrode theory. The surface area can be considered the effective electrolyte-electrode interface rather than the electrode area, estimated from the average particle size of the active material.[21,37] An accurate, effective surface area is difficult to estimate because of the active material particle size distribution, the carbon binder domain, the particles' embedded into the current collector, and the change in particle size during charge and discharge. It should also be noted that the material properties are often considered to be the limitation for diffusion in an electrode. However, the electrode composition and microstructure also impact the observed diffusion.[34] In particular, electrode porosities influence the ability to transport ions to the active material's surface for intercalation. If the pore size is small, this could affect the transport of ions to the materials' surface, particularly at higher current densities. Two electrode configurations using lithium or sodium counter electrodes are often used to extrapolate diffusion parameters. This assumes an insignificant or limited contribution to the counter electrode's observed voltage and diffusion properties, which may not be the case, particularly for plating and stripping.[38,39] These assumptions and estimations make a comparison between reported studies a challenge.[40–42]

In this work, several different electrochemical methods, GITT, EPS, and EIS, are used to determine sodium-ion diffusion characteristics within composite HC electrodes using a 3-electrode cell set-up. The techniques are used to calculate diffusion coefficients; comparisons are reported, and each approach's characteristics are discussed, including the relative advantages and limitations.[18,19,28–31] A third electrode or reference electrode is used to overcome some limitations and assumptions.[34,38,43] This means that the diffusion parameters related to the HC working electrode only can be elucidated, and the polarization contribution of the counter electrode is removed. Test parameters with low current densities are utilized to limit the effect of pore sizes on the diffusion properties. Pulse times are short enough to reduce the effect of any small particles being fully sodiated before the larger particles and

long enough to ensure that a steady-state for sodiation is reached, and the electric double layer's contribution is minimized.

2.1. Galvanic intermittent titration technique GITT.

As introduced by Wen *et al.*, conventional GITT assumes one-dimensional diffusion in a solid solution electrode, neglecting double-layer charging, phase transitions, charge-transfer kinetics, and Ohmic potential drop.[44] It is a combination of transient and steady-state measurements.[30] For time τ, a constant current I is applied to the system (chronopotentiometry), followed by a relaxation step whilst monitoring the voltage to reach equilibrium. The electronic resistance is evaluated over the completed SoC from the instantaneous IR increase when current is applied or removed, and therefore any effect of polarisation or overpotential is negated.[12,32,45–47] With the assumption of small currents and short time intervals, the transient response of the voltage E is a linear function of the square root of time. Hence, the apparent diffusion coefficients $\widetilde{D}_{GITT}$ of the sodium-ions can be obtained by using the **Equation 1**.

$$\widetilde{\boldsymbol{D}}_{\boldsymbol{GITT}} = \frac{\boldsymbol{4}}{\boldsymbol{\pi\tau}}\left(\frac{\boldsymbol{m_{AM}V_M}}{\boldsymbol{M_{AM}S}}\right)^{\boldsymbol{2}}\left(\frac{\boldsymbol{\Delta E_S}}{\boldsymbol{\Delta E_t}}\right)^{\boldsymbol{2}}, \text{ with } \boldsymbol{\tau} \ll \frac{\boldsymbol{L^2}}{\widetilde{\boldsymbol{D}}}. \quad (1)$$

τ is the time interval of the current applied (300 s), m_{AM} the electrode specific mass of active material (g), V_M the molar Volume (48 $cm^3\ mol^{-1}$)[48], M_{AM} the atomic weight of the active material (C_6 = 72 g mol^{-1}), and S is the effective surface area (S = 49.8 cm^{-2}) as estimated from the surface area of the active material in the electrode [21]. ΔE_s is the change in steady-state voltage, and ΔE_t is the change in cell voltage, which can be obtained by inspection of the potential/time plots (**Figure 1**).

The diffusion length L of the sodium-ions depends on the composite electrode characteristics such as porosity and particle size of the active material. Assuming minimum diffusion of L is 4.5 µm (= radius of the spherical particle) and the maximum is ~100 µm (= thickness of the electrode coating in case of for dense electrodes), an apparent diffusion coefficient between 10^{-9} and 10^{-13} $cm^2\ s^{-1}$ can be estimated, hence a time interval of τ = 300 s fulfils the requirement for **Equation 1**.[22,37] It should be noted that these assumptions are not valid for two-phase regions of phase-transforming materials as, within a two-phase region, ions are transported by

movement through the interphase boundary and by ionic diffusion.[45,49] Therefore, the calculated diffusion coefficients are *apparent*, reflecting the characteristics of the whole composite electrode system taking into account the phase change in going from a sodium-poor to a sodium-rich state (sodiation of HC) and vice versa (desodiation).

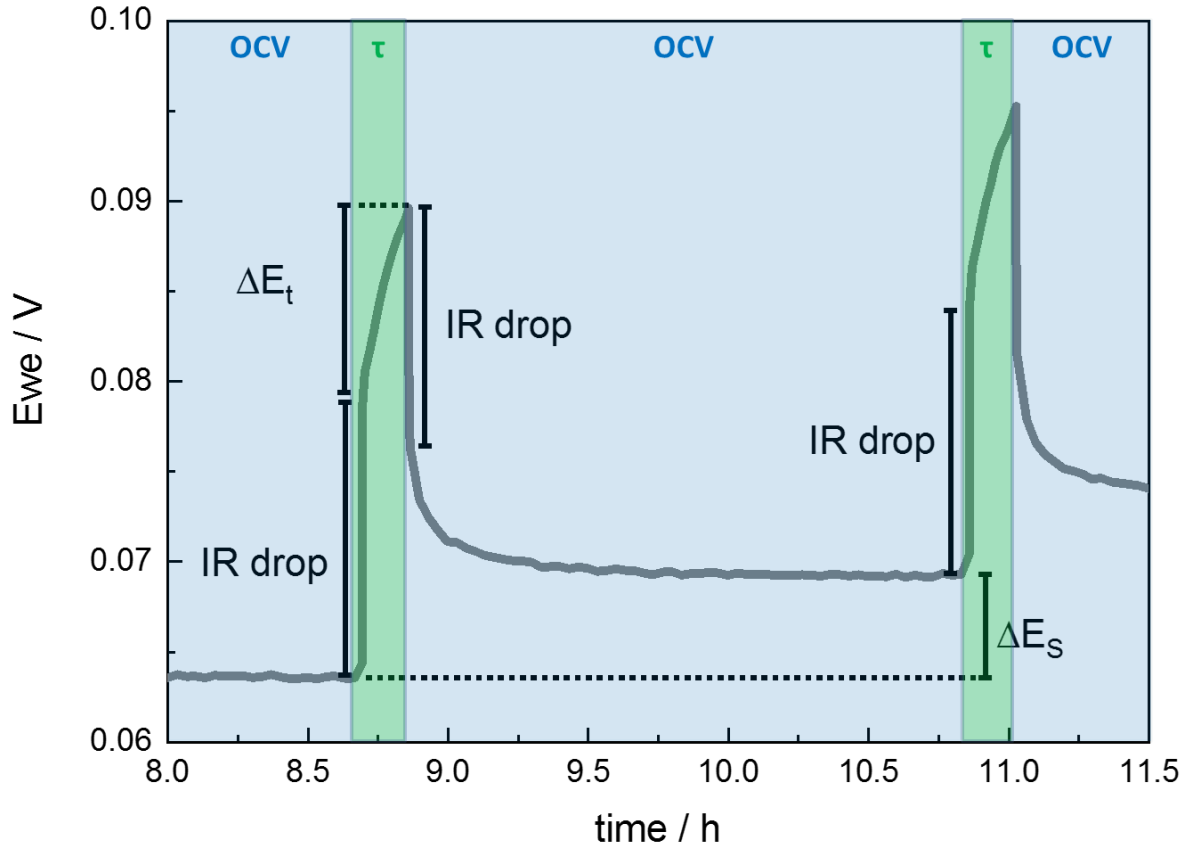

Figure 1. Illustration of two GITT steps (current region "τ" and relaxation region "OCV") showing the working electrode potential E_{WE} versus time. The graph visualizes the voltage drop from polarization (IR), steady-state voltage ΔEs change, and cell voltage ΔE_t.

2.2. Electrochemical Potential Spectroscopy EPS

EPS is a voltage-step technique based on the PITT, skipping the open circuit voltage steps.[28,50–53] In both techniques, a repeated small step increase (or decrease) in voltage is applied, and the current transient is monitored (chronoamperometry). The difference between PITT and EPS is that OCV is not reached between each pulse in EPS, and the pulse duration is limited by current rather than time. To ensure insignificant IR contribution (or overpotential); the minimum current value is chosen close to the thermodynamic equilibrium (e.g., 0.01 C).

The diffusion-limited current is proportional to $t^{-½}$, and the apparent diffusion coefficient can be calculated using the Cottrell equation (**Equation 2**).[44]

$$\boldsymbol{i(t)} = \frac{\boldsymbol{nFSD_{EPS}^{1/2}c_{Na}^{*}}}{\boldsymbol{\pi^{1/2}t^{1/2}}}. \quad (2)$$

c^*_{Na}=c_S-c_0 describes the concentration difference (mol cm^{-3}) between the concentration c_0 in the electrode corresponding to equilibrium voltage and c_S at the electrode-electrolyte interface when a voltage step is applied at t=0. n is the number of electrons transferred per mol of material (1), F is Faraday constant (A s mol^{-1}), and S is the electrode-electrolyte surface area.

For short time approximation ($t \ll L^2D^{-1}$), the chemical diffusion coefficient can be determined from the slope of the linear plot of I vs. $t^{-\frac{1}{2}}$ by **Equation 3**.

The slope of each current decay is proportional to $D_{EPS}^{1/2}$ provided that the concentration difference c^*_{Na} is known. The equation can be rearranged for capacity change (ΔQ) and assuming a spherical particle of radius r.

$$\boldsymbol{i(t) = nFSc_{Na}^{*}\sqrt{\frac{D_{EPS}}{\pi t}} = \frac{3DQn}{r}\sqrt{\frac{D_{EPS}}{\pi t}}} \quad (3)$$

Assuming a diffusion length of 4.5 µm (radius of spherical hard carbon particle) and an apparent diffusion coefficient between 10^{-10} to 10^{-16} [18,33,54], the experimental parameters meet the condition for short time approximation, $t \ll L^2D^{-1}$ with $t \ll 2025\ s$.

2.3. Electrochemical Impedance Spectroscopy EIS.

EIS is used to investigate electrochemical systems by separation of processes with different time constants.[37,47,55–59] As the battery processes occur at different rates, the system's response can be divided into different sections. The low-frequency region of EIS is associated with solid-state diffusion from which apparent diffusion coefficients can be extracted. EIS is conducted by applying an oscillation current (galvano-EIS, GEIS) or potential (potentio-EIS, PEIS) to a system and recording the phase and amplitude response. The potential or current stimulus should be low enough to keep the system within a quasi-stable state and a quasi-linear part of the voltage curve but high enough for adequate signal-to-noise discrimination. The

potential profile of the electrode can be used as an indication. For example, within the plateaus of the voltage profile, even a small potential stimulus induces a SoC change. For a classical Warburg response, the diffusion must be semi-infinite, planar and adhere to Fick's law of diffusion, which is a purely concentration gradient driven ionic transport process.[55,58,60] If these assumptions hold true, then the diffusion coefficient $\widetilde{D}_{EIS}$ can be calculated from the Warburg coefficient (σ).[42,53,61] To check whether the correct conditions are reached, the phase angle for the Warburg coefficient should be 45° (D∝√L). In most porous electrodes, this condition is not met, hence the assumptions are not valid. A transition line equivalent circuit model, which includes finite diffusion of the lithium-ion in a solid hard carbon particle and the electrolyte within the pores, has been used previously to fit the impedance data.[62,63] At the higher voltages (>1.3 V vs Na/Na^+), where there is no sodium in the carbon, no charge transfer is observed, and the resistance from the pore network can be extrapolated. At the lower voltages, the electrode is in a non-blocking condition. At the higher voltages, the impedance can be fitted with a modified Warburg coefficient equivalent circuit element for finite diffusion (M_a) or anomalous diffusion (M_g).[64] The ionic transport in the pore network can be investigated using **Equation 4** where γ = 1 for M_a. R_s is the series resistance, and the exchange current density can be estimated from the contributions of the charge transfer resistances R_{CT} using **Equation 5**.

$$\frac{1}{\tau_c} = f_c = \left(\frac{D_c}{L_c^2}\right)^{\frac{1}{\gamma}} \quad (4)$$

$$j_0 = \frac{R\,T}{R_{ct} F\, S_{eff}} \quad (5)$$

3. Experimental

3.1. Electrode preparation and cell building.

The HC composite electrodes compromise a commercial HC material (D50: 9 µm), polyvinylidene fluoride (PvdF, Kynar, HSV900) and carbon black (TimCal, C45) in a 90:5:5 wt. % ratio. N-methylpyrrolidone (NMP) was used to formulate an ink with a solid content of approximately 42 %. The ink was coated onto a carbon-coated aluminium current collector using the doctor blade method. The electrodes had a mass loading of 110 g cm^{-2} (coat weight). The pre-dried (infrared exposed) electrodes were placed into a vacuum oven at 120 °C

for at least 90 minutes to remove any NMP residues. The dried electrodes were calendared to 35 % porosity with calculations based on the density of the composite electrode materials and the dry coating volume (electrode surface × thickness). The same electrode coating was used in all three electrochemical tests.

All experiments were performed in a 3-electrode cell set-up based on a compression fitting design. The current is applied between the working and counter electrode, whereas the working electrode potential is recorded versus the reference electrode to insulate the working electrode performance from the overall cell performance. HC composite electrodes with 11 mm and 12 mm diameter were used as working electrodes and transferred into a glove box. All following cell preparation and assembling was conducted in an argon atmosphere. Sodium metal was used as a counter and a reference electrode, respectively. Therefore, a clean sodium ingot was flattened to approximately 0.5 mm in thickness. 10 mm sodium metal discs were punched out for the counter electrode, and the T-piece attachment of the 3-electrode cell was filled with the flattened sodium metal. Counter and the working electrode were separated by combining one GF/A Whatman and one 20 µm polypropylene (PP) separator (2020, Celgard). A similar separator stack was placed perpendicular to the cell stack for electronic insulation of the reference electrode. The combination of separators was used to ensure cycle stability (thick glass fibre separator reduces the risk of inner short circuits due to dendrite growth) and avoid contamination of glass fibres on the HC electrode to facilitate post-mortem analysis (thin PP separator facing towards the working electrode). A total of 130 µl of a premade electrolyte containing 1 M $NaPF_6$ in a 1:1 (v) mix of ethylene carbonate (EC) and diethylene carbonate (DEC) (Kishida Chemicals) was used as an electrolyte to wet both separator stacks.

3.2. Electrochemical measurements.

The connection set-up was kept identical for all testing methods. The current was applied between the counter and the working electrode, whereas the electrode potentials were monitored via the reference electrode. The cut-off conditions for the constant-current charge and discharge were based on the working electrode potential.

GITT was performed using a BaSyTec cell tester (CTS system, 1 µs time resolution, 0.05 µA current resolution, 0.3 mV voltage resolution). EIS and EPS were conducted using a Bio-Logic potentiostat (VSP model, 200 µs time resolution, 760 pA current resolution, 5 µV voltage resolution). One full cycle at 0.2 C using an assumed capacity of 330 mAh g^{-1} was conducted as formation before performing GITT and EPS measurements. During formation, the cell was discharged in constant current/constant voltage (CCCV) mode, with a cut-off voltage of 0.005 V and a current of 0.01 C (sodiation process). Charging was conducted using a constant current (CC) at 0.2 C up to 1.5 V (desodiation process).

For GITT, a current of 0.2 C was applied for five minutes, followed by an OCV step with a termination condition based on a working electrode potential variation of $\Delta E_{WE} \leq 0.001$ mV s^{-1}. This termination parameter is essential to ensure a quasi-equilibrium state as ongoing diffusion processes and polarization affect the results.[38] Subsequent cycling was performed using identical parameters as for the formation cycle.

EPS was conducted in 10 mV potential steps monitoring the current decay. The termination condition of each voltage step was a minimum current I_{min} of 0.01 C. A sufficient low cut-off current I_{min} is essential as it ensures a state close to the equilibrium and avoids any influence of polarization effects, as stated earlier. After triggering the termination condition, the working electrode potential was raised by another 10 mV relative to the previous starting value.

The EIS measurements were conducted at 16 evenly spread potential steps within sodiation and desodiation, respectively. A 150-minute OCV step followed each potential step to ensure full relaxation of the electrode to reach the equilibrium state before conducting the EIS measurement. For EIS, a spectrum of 52 frequencies between 50 mHz and 1000 kHz were chosen, applying an amplitude of 2 mV and recording the average impedance based on three measurements per frequency. A low amplitude was chosen to minimize the contributions of SoC changes within the low plateau region. All electrochemical measurements were conducted at room temperature.

In the calculated diffusion coefficients discussed below, we have utilized an effective surface area (S) related to the active electrolyte-electrode area of 49.8 cm^{-2}, based upon an electrode coat weight of 110 gsm, the porosity of 35 %, and an average hard carbon particle of 9 µm

(calculation based on spherical particles with a radius of 4.5 µm). When using the geometrical electrode area (A=1.131 cm^{-2}), as also stated in the literature, the diffusion coefficient would change by a factor of 4×10^4 cm^2 s^{-1}; this should be considered when comparing results to literature.

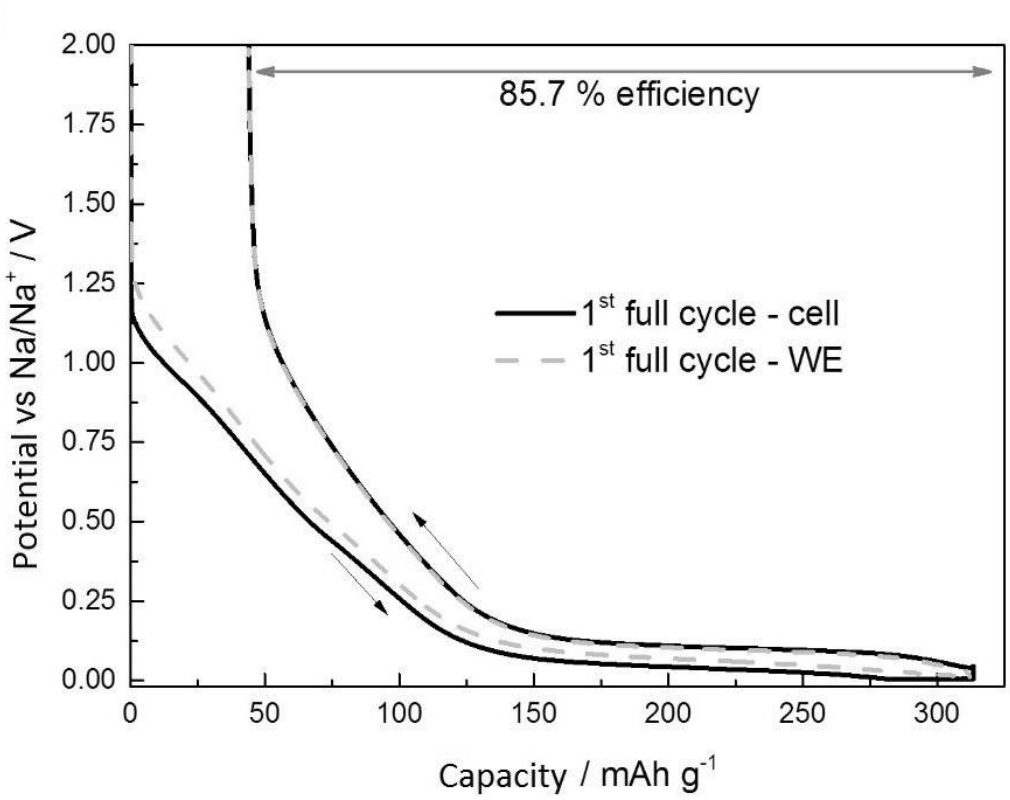

Figure 2. Full formation cycle of an HC half-cell showing the working electrode (WE) potential (HC vs Na metal reference) compared to full-cell potential (WE vs counter electrode, CE) and the first cycle efficiency.

4. Results and discussion

4.1. Results and discussion of the formation cycle

All electrochemical tests start with a formation cycle to assure good cycling properties and create the electrolyte-carbon interface layer. Hereby, characteristics such as initial capacities, first cycle losses, and reference connections can be checked. An example of the formation, the first cycle of one cell, is shown in **Figure 2**. The graph displays the working electrode potential (dashed line, E_{WE}) and the cell potential (straight line, cell, measured between the working and counter electrode). A mismatch between the E_{WE} and cell potential can be seen during sodiation

caused by the polarization on the sodium metal counter electrode.[38] The HC electrode shows an initial sodiation capacity of approximately 330 mAh g^{-1} and a first cycle efficiency of approximately 85 %, consistent with the literature.[6,11,17,31,65,66]

4.2. Results and discussion of GITT measurements

The GITT measurements were performed in the second and 10^{th} cycle after an initial formation cycle to investigate the influence of cycling on ionic mobility using a 3-electrode cell set-up. A full GITT cycle showing the sodiation and desodiation branch of an HC working and sodium metal counter electrode is shown in **Figure 3**. The series of sodiation and desodiation steps, each followed by an OCV step, can be observed in Figures (a) and (b), respectively. The length of the OCV steps varies depending on the SoC and potential of the WE. The same data, the working and counter electrode's voltage profile, plotted versus the capacity is shown in (c) and (d). The polarization of the sodium metal counter electrode during sodiation and desodiation is clearly seen. The polarization depends on the SoC of the electrode and is approx. double during sodiation compared to desodiation.

The apparent diffusion coefficients were calculated using **Equation 1** in a voltage range between 1.2 V and 5 mV, and the results are shown versus the capacity in (e) and (f)**.**

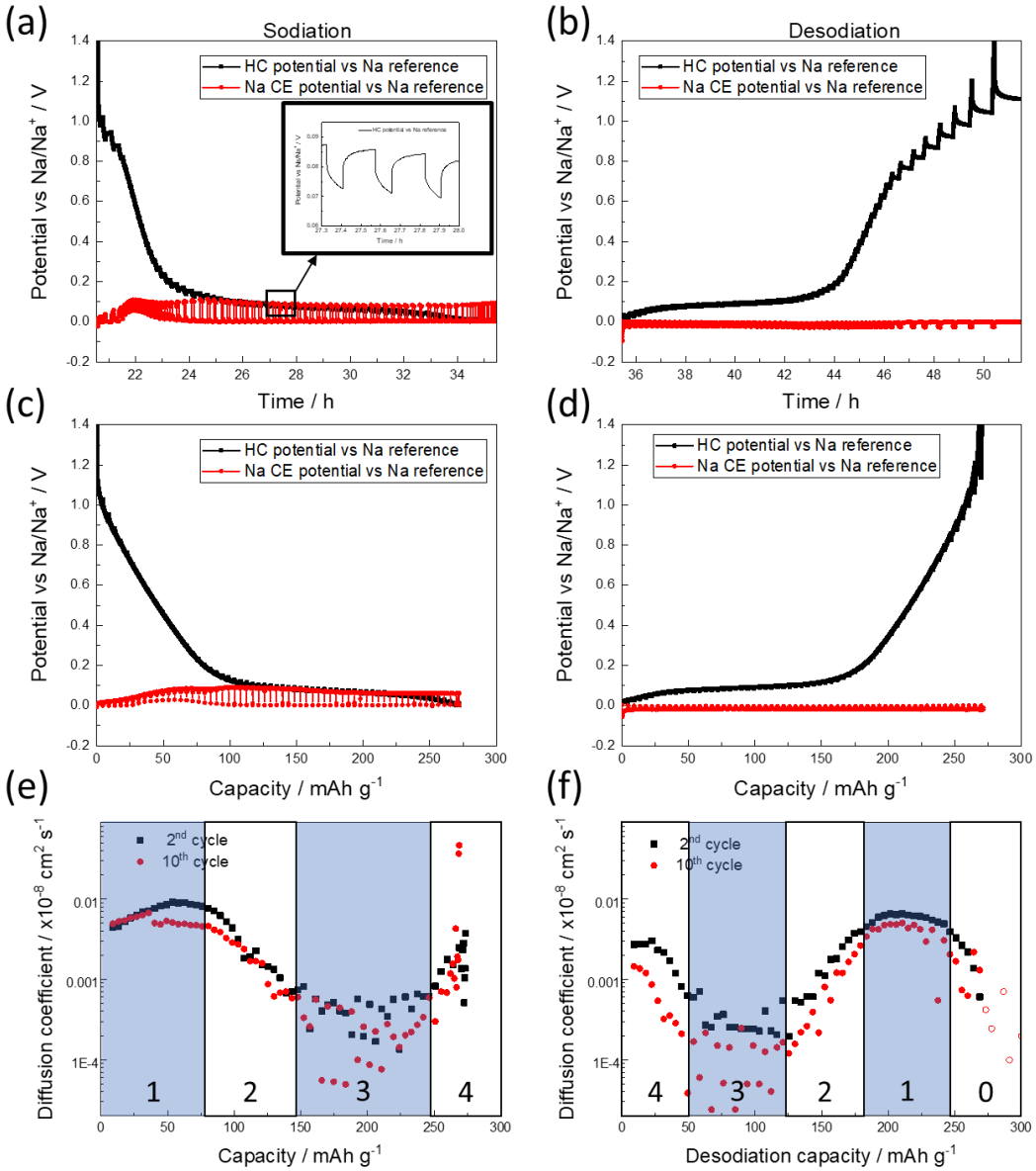

Figure 3. GITT profile of the sodiation (left) and desodiation (right) branch of the HC working and sodium metal counter electrode versus time. (a) and (b) show the potential curve versus testing time, (c) and (d) show the potential versus capacity. (e) and (f) show the corresponding apparent diffusion coefficients during sodiation (left) and desodiation (right) within the second (squared marker) and 10^{th} cycle (circular marker) determined from 3-electrode GITT measurements. Coat weight of 13.5 mg.

The apparent diffusion coefficients' values vary by at least one order of magnitude for all four profiles. In the second sodiation, minimum values of around 5×10^{-12} cm^2 s^{-1} and maximum

values of around 1×10^{-10} cm^2 s^{-1} are determined. The profile for the second desodiation is revered, and the values are lower compared to the sodiation (minimum around 3×10^{-12} cm^2 s^{-1}; maximum around 8×10^{-11} cm^2 s^{-1}). A general decrease in the diffusion coefficient is apparent for the cycled electrodes. The cycled electrodes' profiles appear noisier with a prolonged plateau region (minimum around 2×10^{-12}; maximum around 7×10^{-11} cm^2 s^{-1}).

All profiles of the apparent diffusion coefficient can be divided into four and five regions, respectively. For sodiation, the values are plateau-like for the first 100 mAh g^{-1} (region 1), followed by a decrease of one to two orders of magnitude (region 2) to a second plateau from around 150 to 250 mAh g^{-1} (region 3). For both sodiation cycles, the values increase slightly at the end of sodiation from 250 and 270 mAh g^{-1} onwards (region 4), respectively. The profile for the apparent diffusion coefficient values for the second desodiation is mirrored to that of the sodiation (region 4 → 1). An additional region (region 0) can be distinguished as the values drop at the end of desodiation by one order of magnitude (**Figure 3** (f)). A similar performance can be seen for the 10^{th} sodiation for regions 4 to 0.

Ionic mobility within battery materials is essential for the overall battery performance. Hence, apparent diffusion coefficients for HC electrodes based on GITT experiments have been reported in the literature before with maximum values between 10^{-11} to 10^{-8} cm^2 s^{-1}. [19,25,26,37,38] The results differ based on the parameters and settings used; for example, testing in 2- versus 3-electrode arrangement and varying the length of the OCV step to achieve an equilibrium. Further, the parameter setting for *S* differs, as often the geometrical surface, and BET surface or numbers of approx. calculation based on porosity and particle size is used. Although the mentioned parameters influence the absolute values, the shape of the diffusion curve is similar, and so are the shown graphs in Figure 4 in accordance with published data.

The mirrored profiles for sodiation and desodiation for GITT values indicate a reversible process for the second cycle. The variation of the apparent diffusion coefficients within each sodiation and desodiation cycle points out a strong dependence on the SoC, with a correlation of the low plateau region of the apparent diffusion coefficient to HC's low voltage potential. The presented stepped voltage profile of the GITT curve (Figure 3) suggests different stages for ionic diffusion within the sodiation and desodiation process, which correspond to the

diffusion coefficient changes. Plateau regions might indicate semi-stable diffusion characteristics (regions 1 and 3), whereas regions of fast decreasing or increasing values suggest changes in the diffusion characteristics (regions 2, 4, and 0), and hence a change in the sodiation mechanism.

The voltage transient at low voltages is not linear at the end of the pulse, making the diffusion coefficient more difficult. The non-linearity indicates that the processes occurring in the material and electrode are non Fickian. Hence, the calculated values at low sodiation potentials are less conclusive. Besides, as the plating potential is reached, no or limited diffusion occurs in the active material. Additionally, this could indicate that the sodium metal 'pooling' in the hard carbon at the low voltages is not limited by the intercalation but the formation of the nano-clusters of sodium and that at these low voltages, sodium could plate onto the surface of the electrodes.[16,20,67]

Measurements of the diffusion coefficients at higher potentials were difficult due to the high polarization at those potentials, which triggered the cut-off voltage limitation at desodiation. This polarisation is expected as the sodium concentration is very low in the hard carbon at these voltages resulting in a lower overall electronic conductivity in the composite electrode.

4.3. Results and discussion of the EPS measurements

EPS measurements were conducted in a 3-electrode cell set-up after an initial formation cycle. The EPS profile for the working electrode, the counter electrode (sodium metal), and the monitored cell current is plotted in **Figure 4.** The graphs show the profiles for sodiation (left) and desodiation (right). The working electrode potentials (upper graphs) show the staircase profile of the 10 mV voltage steps. The polarization of the counter electrode at each voltage step can be seen in the middle graph. During sodiation of the hard carbon working electrode, the counter electrode's polarisation increases towards lower potentials; during desodiation, the polarization decreases towards higher potentials and vice versa. The polarization shows a maximum of around 8 mV within the low plateau region of the HC potential (middle graphs). The bottom graphs show the current profile monitored during sodiation and desodiation. Each

voltage step is accompanied by an exponential current decay due to diffusion processes.

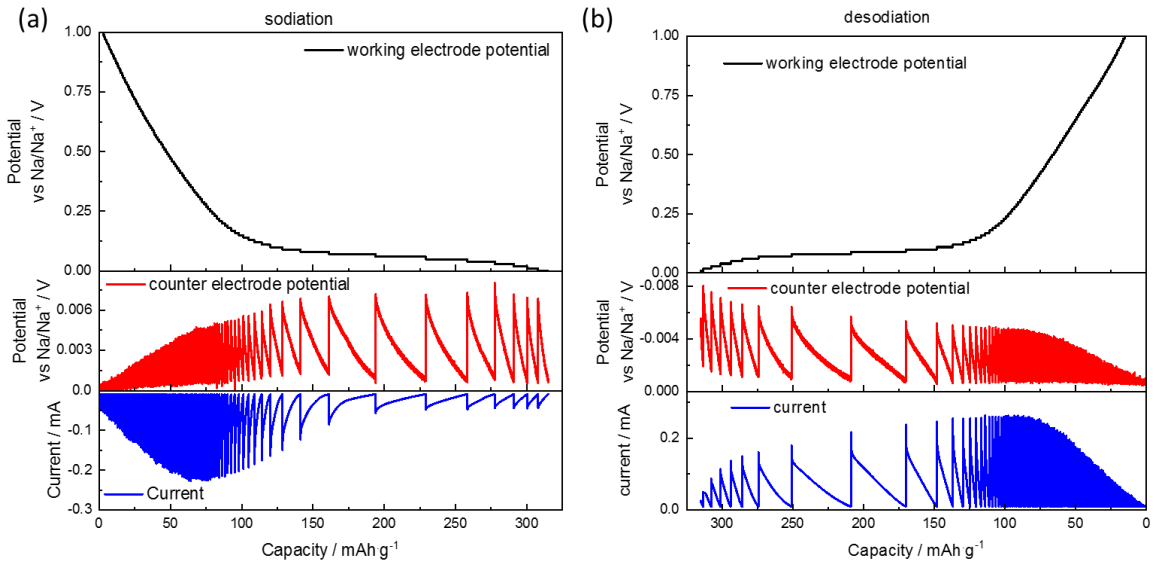

Figure 4. Working (HC), counter (Na metal) electrode potential and current profile of the EPS cycle for sodiation (left) and desodiation (right) of an HC composite electrode versus the gravimetric capacity (active material based). Coat weight 12.8 mg.

As an additional remark, **Figure 4** also highlights the importance of a three-electrode set-up as the sodium counter electrode's potential varies between 6 mV and -8 mV at sodiation and desodiation, respectively. Calculations based on the cell voltage profile may lead to inaccuracies in the diffusion coefficient's calculated values.

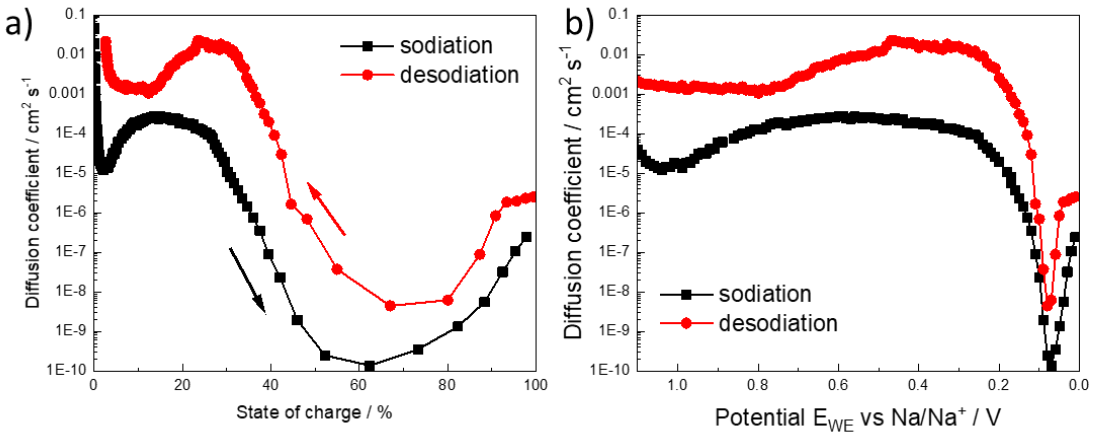

Figure 5. Apparent diffusion coefficients based on EPS data for sodiation (black square) and

desodiation (red triangle) of the 2nd cycle plotted versus the SoC (a) and working electrode potential (b).

Apparent diffusion coefficients were calculated following **Equation 3** using a linear fit for the current *i(t)* versus the time $t^{-½}$, with the slope of each current decay being proportional to D_{EPS}. The results are plotted in **Figure 5.** It displays the calculated apparent diffusion coefficients based on the EPS measurements for sodiation and desodiation versus the SoC. The values of the apparent diffusion coefficient change by three orders of magnitude during sodiation and desodiation. For sodiation, the values start at a high level (7×10^{-8} cm^2 s^{-1}) and decrease, undulating to around 0.03×10^{-8} cm^2 s^{-1} when 100 % SoC is reached. The first decrease to 0.2×10^{-8} cm^2 s^{-1} appears within the 0 to 3 % of SoC. This is followed by a rise of the values to around 0.8×10^{-8} cm^2 s^{-1} at 20 % SoC and a subsequent drop with its minimum at around 60 % SoC. The lowest values can be found between 50 and 80 % SoC (0.006×10^{-8} cm^2 s^{-1}). The desodiation profile is in reverse, showing slightly increased values between 100 and 20 % SoC. The profile of the apparent diffusion coefficient appears similar for sodiation and desodiation, suggesting a reversible process. The changes in diffusion during the sodiation and desodiation process indicate at least a two-step process. Again, one step within the sloping region of the voltage profile and a second one within the plateau region, as described and discussed above.

Based on the test plan's set-up, the data points of the apparent diffusion coefficient are not equidistant when plotted versus the SoC (capacity). Since the measurements are taken in equidistant voltage steps, and the characteristic voltage profile of the hard carbon consist of a sloping and a plateau region, the data density is much higher at low SoC (sloping) compared to higher SoC (plateau). This leads to a high resolution between approx. 0 to 30 % SoC, followed by a few data points between 40 and 80% SoC (plateau region).

4.4. Results and discussion of the EIS measurements

EIS was conducted in the first, second and tenth cycle using a 3-electrode cell set-up. Within each sodiation and desodiation cycle, 16 EIS spectra (equidistant voltage steps) were generated to cover the full range of SoC. **Figure 6** shows the 16 EIS spectra for sodiation (left) and desodiation (right) in a voltage range between 1.7 V and 5 mV for the 2nd cycle. Differences in

the shape of the Nyquist plots at various SoC indicate changes in resistance, capacitance, surface layer formation, and pore sizes changes.[57,66,68–70] Further, the low-frequency branch's appearance, which reflects solid-state diffusion impedance, changes with the SoC. The series resistance also changed with SoC. The resistances shown are between 5.1 and 6.7 Ω for the 2nd cycle and increased to between 7.7 and 9.3 Ω for the 10th cycle. In all cases, the charge transfer resistance (R_{CT}) was only visible at voltages less than 1.1 V vs Na/Na^+, and the EIS plots indicate an ion blocking arrangement. The phase angle at these low frequencies at the higher voltages is greater than -60, indicating a pseudocapacitance effect. The charge transfer R_{CT} can be mapped from 1.1 V to 0.005 V vs Na/Na^+.

We can, however, use the data to fit R_{CT} and calculate the exchange current density for hard carbon over all states of charge.

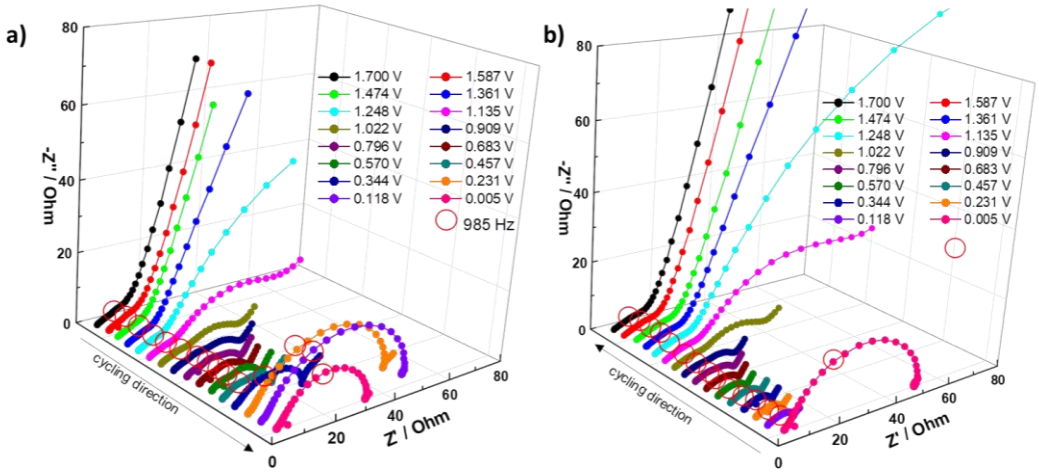

Figure 6. EIS spectra versus voltage for the full second sodiation (a) and desodiation (b) between 0.005 and 1.7 V. Data was recorded between WE and reference electrode in a 3-electrode set-up. Electrode coat weight: 13.8 mg.

From the high voltage data (>1.4 V vs Na/Na^+), the data can be assumed to be in an ion blocking state and using the transition line model, the resistance with respect to the pore network can be calculated, and no charge transfer resistance is observed.

As an example, and to visualize the influence of aging on the electrode performance, **Figure 7** shows the EIS spectra at 0.457 V for the second cycle (a) and tenth cycle (b) displayed in the Nyquist plot. The graphs show a higher overall impedance R_{CT} for the sodiation compared for desodiation (second cycle: 20 to 14 Ω; tenth cycle: 150 to 87 Ω) as well as an increase in impedance during cycling (sodiation: 20 to 150 Ω; desodiation: 14 to 87 Ω). The differences in sodiation, desodiation, and age of the electrodes can be seen in the angle and frequency shift of the low-frequency region. Hence, Figure 7 (c) and (d) shows the Bode plots based on the same data. The increase in the overall impedance is also seen in Figure 7 (c), highlighting the pronounced effect for lower frequencies. Also, the impedance profile of sodiation and desodiation diverge for frequencies above 1 kHz. Within the phase diagram in Figure 7 (d), two distinctive local minima and two local maxima can be determined for the sodiation curve,

whereas the desodiation branch shows less distinct features.

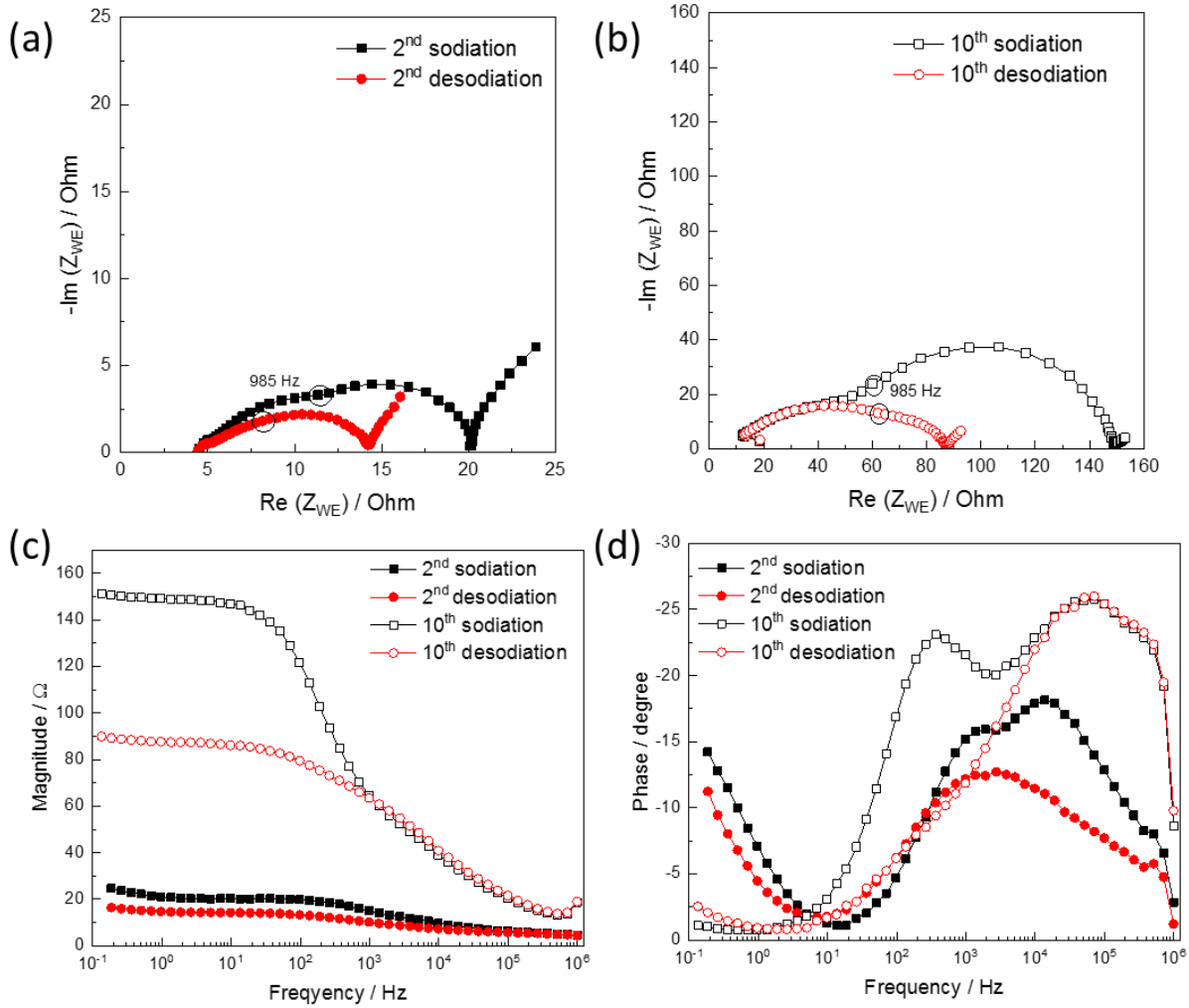

Figure 7. Impedance data of the second and tenth sodiation and desodiation at 0.457 V.

The impedance for sodiation is higher than the impedance for desodiation at all frequencies. Upon the 10th cycle, the significant difference is likely due to the blocking of the pores in the electrode by an SEI layer. **Figure 7 (d)** shows the change in phase at different frequencies; two peaks in the 2nd cycle desodiation are observed at 1KHz and 10kHz. Upon the 10th cycle, these appear to shift to 100 and 100kHz. This shows that the two transport mechanisms, likely relating to the transport of the ions through the interface and the sodiation of the hard carbon, are increasing.

The exchange current density (j_0) and the effective diffusion can be calculated from the equivalent circuit. Where possible, the data were fitted with an equivalent circuit model

including an anomalous diffusion element, the exchange coefficient is calculated from the charge transfer resistance, and the change from the 2nd to 10th cycle is shown in **Figure 8**. There is a significant difference in exchange current density between sodiation and desodiation, with a maximum during desodation around 150 mAh g^{-1} of 5 x 10^{-5} A cm^{-2}.

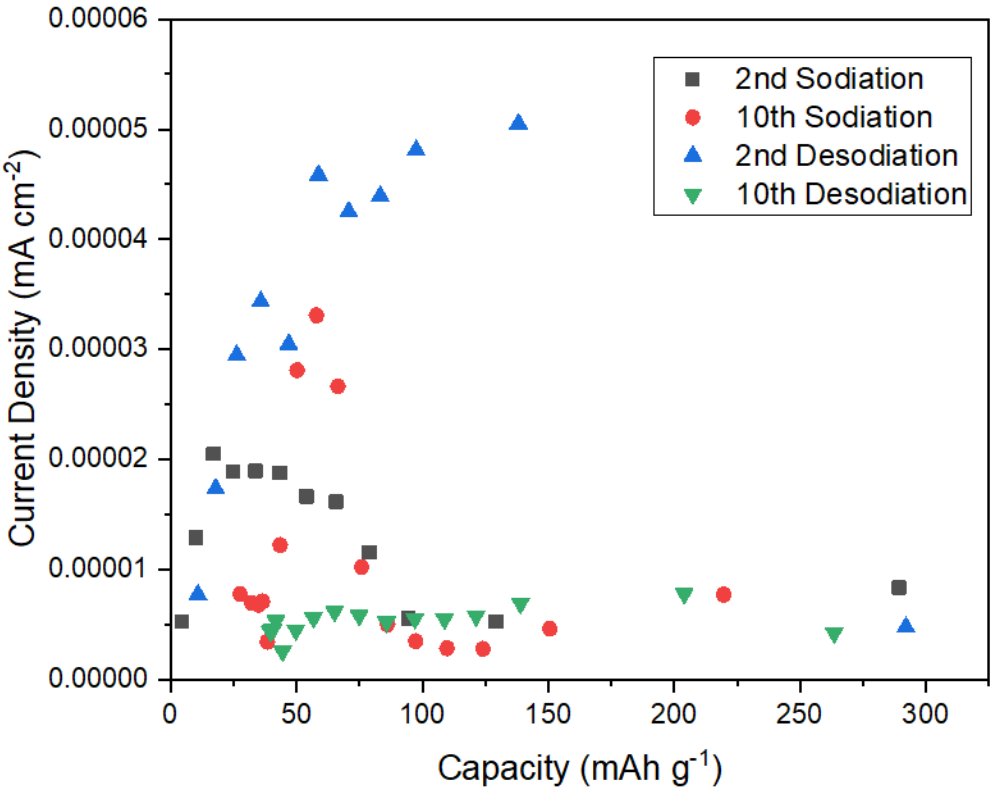

Figure 8. Exchange current density for the 2nd and the 10th cycle.

To analyze the diffusion characteristics, the focus for the EIS measurements is on the low-frequency region, which relates to the diffusion in a solid. Here we fit the tail with an anomalous diffusion element M_g and calculated the diffusion coefficient according to **Equation 4** (results shown in Supplementary Information (**Table S1**)). **Figure 9** shows the calculated diffusion coefficients versus the SoC of the composite electrode for sodiation (left) and desodiation (right). A similar trend to that observed from the GITT and EPS was measurements was observed, with an increase in diffusion coefficient in the first 50% state of charge. Gaining

accurate data for the higher specific capacities at low voltages was difficult, as there were limited data points, and the fitting was difficult due to overlapping transport mechanisms occurring at low frequencies.

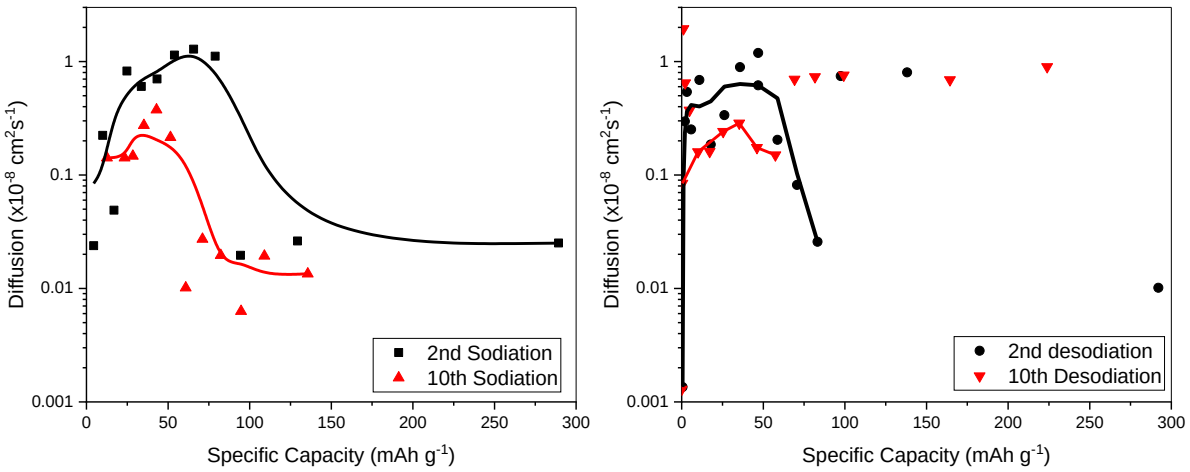

Figure 9. Apparent diffusion coefficients are plotted versus the SoC, based on low-frequency impedance data for sodiation (left) and desodiation (right) of the 2nd and 10th cycle.

Publications on apparent diffusion coefficients gained from EIS data are rare in the literature. EIS is mainly used to investigate the diffusion in cathode materials as the crystal structure changes during charge and discharge.[58,60,71–74] It should be noted that the resolution within the low voltage region is very low when conducting staircase PEIS. Additionally, the data acquisition is not as accurate within the low voltage plateaus. The variation in voltage changes the SoC, and then the requirement for the semi-stable condition is not fulfilled. In future, rather than controlling the sodiation by voltage, it is recommended to control the sodiation by coulomb counting. This should reduce the observation of sodium plating at the low potentials and provide greater accuracy in the low voltage region. Using galvanostatic EIS would lead to more reliable results in the low voltage plateau. However, it would cause inaccuracy for the diffusion coefficient calculation as even a low applied current amplitude would lead to a SoC change at low frequencies, which are needed for the diffusion coefficient calculation. In this study, PEIS was chosen to gain more information in the sloping voltage

region of the hard carbon to complement the information obtained through the GITT measurement.

4.5 Discussion

The minimum and maximum actual diffusion coefficients for each technique were orders of magnitude different. However, for all techniques, the apparent diffusion coefficients indicate a reversible sodiation and desodiation, respectively (GITT: Figure 3, EIS: Figure 9, EPS: Figure 5). The values decrease with aging, whereas the differences between fresh and cycled cycles are most significant in the plateau region of the HC sodiation/desodiation profile (130 to 220 mAh g^{-1}, 35 to 85 % SoC). Bommier et al. attribute this effect to cell degradation resulting in hindered ion diffusion within the cell.[75] We have shown previously that the change in diffusion upon cycling and the increase in resistance are due to reduced pore networks within the electrode. The pores become blocked with SEI growth, limiting the transport of electrolyte and ions to the material's surface.[35,76] The voltage range covered by the apparent diffusion coefficients differs slightly due to the different techniques used. It is also important to note that the EIS data's resolution (16 data points per sodiation) is lower than for the GITT data (64 data points per sodiation). Both illustrations were chosen as the graph versus the SoC is beneficial as GITT measurements are based on capacity intervals, whereas the EIS measurements were performed in voltage step intervals. The mechanisms and apparent diffusion coefficients correspond well to those reported previously in the literature, Table S2.[7,20,67,77,78] Three distinct storage mechanisms are observed:

1. Capacitive and redox-active surface charge storage ((>1.3 V vs Na/Na^+))
2. Intercalation (0.1-1.3 V vs Na/Na^+) and
3. Metallic or quasi-metallic deposition (<0.1V vs Na/Na^+).

At intermediate voltages, it is likely that the different storage mechanisms are observed simultaneously. At high voltages (>1.3 V vs Na/Na+), capacitance is observed in EIS, as the time constant is $\propto 1/t$. EPS shows high diffusion coefficients at these very low capacities. As the voltage decreases to ~0.15 V vs Na/Na+, intercalation starts to occur, and the diffusion coefficient increases to a peak at approximately 75 mAh g^{-1} at which the EIS has a phase angle

of approximately 45° at 0.457 V vs Na/Na+ indicating a time constant for diffusion is $\propto 1/\sqrt{t}$. The diffusion coefficient then steadily decreases to a minimum at 200 mAh g^{-1}, which subsequently increases to full sodiation (~300 $mAhg^{-1}$). From the change in low-frequency phase angle at these corresponding sodiation voltages, it is apparent that there are likely mixed transport mechanisms occurring. These observations correlate very well with the mixed mechanisms proposed by Au *et al.*[77]

We have also shown that the counter electrode resistance increases with cycling, affecting the measurements, particularly in 2-electrode measurements.[38] The use of 3-electrode cells means that the effect of the counter electrode can be largely ignored. When comparing the range of the apparent diffusion coefficient values, it is noticeable that the values based on GITT measurements change within two orders of magnitude, whereas the values for EIS change by four and EPS by six orders of magnitude. Nevertheless, the shape of the sodiation and desodiation profiles of the apparent diffusion profiles based on GITT end EPS look similar.

Table 1 lists the accounted parameters needed to evaluate the apparent diffusion coefficients for each technique presented. In all methods, the derivation of the method is based upon Fick's law of diffusion. Therefore if the sodium ion transport mechanism deviates from the assumption that sodium concentration change $\propto \sqrt{t}$ at each data collection time period, the calculations for diffusion coefficient will not hold true.

Table 1. List of parameters for evaluating the apparent diffusion coefficient for the three techniques used: GITT, EIS, and EPS.

	GITT	EIS	EPS
Controlled via	Current	Potential	Potential
Time constant	$V(t) \propto \sqrt{t}$	$I(t) \propto \sqrt{t}$	$I(t) \propto \sqrt{t}$
Step limitation	$\Delta E_{WE} \leq 0.001$ mV s^{-1}	150 min OCV	I < 0.01 C
mathematical parameters (constant)	Surface Pulse time $\boldsymbol{\tau}$ Molar mass Molar volume Active material mass	Surface Temperature	Surface Diffusion length Current (limitation condition)
Over potential (IR)	None	None	Yes, low
Values obtained for analysis	Titration (equilibrium voltages)	Modified Warburg coefficient	Step time Concentration change

	ΔE_s / ΔE_t	Concentration Current	
Total testing time after the second cycle	51 hours	174 hours	69 hours

General aspects:

The important key parameters valid for the whole potential region are: experimental control, step limitation, IR contribution, parameter settings and test duration.

- In all methods, the derivation of the method is based upon *Fick's laws of diffusion*. Therefore, if the sodium ion transport mechanism deviates from the assumption that the sodium concentration changes, the calculations for diffusion coefficient will not hold true.
- The *step/measurement limitations* were chosen to be close to an equilibrium state. The time scales of the sodiation and desodiation steps reach from 1 to 17 minutes for GITT, fixed 150 minutes for EIS, and tens of seconds up to 4.5 hours for EPS. The corresponding currents are 0 mA for GITT (OCV step), < 0.002 C for EIS and < 0.001 C for EPS. The variation strongly depends on the SoC of the electrode and the technique used (see also following paragraphs). In the titration methods, the error relating to the overpotential is reduced due to open circuit voltages being used in the calculations for diffusion, although estimation of the ohmic resistances (IR-drop) is difficult.
- The *measurement control* is via the current (GITT) or the potential (EPS and EIS). When controlled via current, the polarisation effects trigger the step limitations faster. Therefore, the voltage range covered by the apparent diffusion coefficients differs slightly between the different techniques used.
- EIS is a time-intensive method, especially when focussed on the low-frequency region for diffusion analysis. Although EIS shows the lowest data's resolution (16 data points per sodiation) of all three techniques (GITT: 64 data points per sodiation, EPS: 138 data points for sodiation), the *testing time* is three times larger compared to GITT.
- Test cells built on a lab-scale, especially 3-electrode cells, suffer from higher self-discharge or leakage currents via the reference electrode local corrosion and ageing.

This leads to higher capacities during sodiation and lower capacities for desodiation and deficient concentration calculations.

- In this work, the electrodes' porosities were set to 35 %. Therefore the transport in the electrolyte should be similar for all electrodes. During sodiation, the expansion of the material and increase in the interface layer thickness will reduce the pore size, and at low voltages, if sodium deposition occurs, a further reduction in pore size is likely. This also increases the internal resistance and impedes the charge transfer. Here we have assumed the pore fraction is assumed to be constant, the influence of changing diffusion pathways is ignored.
- All test cells were built from the same printed electrode, and an identical cell design was used. Hence electrode related parameters are unlikely to be the cause for the differences.
- In general, the GITT condition of $\Delta E_{WE} \leq 0.001$ mV s^{-1} might be too soft, meaning a true equilibrium is not reached, leading to too high values for ΔE_S, causing an overestimation of the apparent diffusion coefficient. In this case, it may be more appropriate to fit the SAND equation to the voltage transient, as then the variation in reaching OCV would not be taken into account.

Lower voltage region:

Besides the factors discussed above, several potential testing artefacts are arising at different voltage levels for these methodologies. At the low voltage level, these include:

- For GITT at the low voltages, very low diffusion coefficients are observed, and there is little change in the voltage. As the calculation for the diffusion coefficient is reliant upon the change in the voltage, small errors in voltage will make a large difference in the calculated coefficient. If ΔE_t is larger than expected, an underestimation of the diffusion coefficient is observed.
- EIS and EPS were both controlled by voltage rather than current. Therefore, the calculation of the concentration of sodium in the solid is difficult at the low voltage plateau. However, the small changes in voltage in EPS measurements mitigate some

inaccuracies, particularly with the current limiter of 0.001 C. Where the voltage steps induce a large change in sodium concentration, such that $t \gg L^2 D^{-1}$ the equation $D_{EPS} = \frac{dln(I)}{dt}\frac{4L^2}{\pi^2}$ can be used. Even so, only two points across the low voltage region for the EIS measurements do not reflect the complete change in the diffusion coefficient at the low voltage.

- Especially the EIS measurements seem to be affected by processes occurring at very low voltages. It is suggested that within the low voltage region, sodium metal deposits on the HC surface and metal sodium clusters form within the HC's pore space.[15,16,20,48,79] This increases the electronic conductivity of the HC and changes the local sodium concentration (local potential ≠ electrode potential), also causing induction effects from the surface interference.[80,81] The Nyquist plots at low voltages shown in Figure 6 show the lack of a Warburg feature, but induction loops. The Warburg feature is missing during desodiation, indicating a faster sodium transport away from the surface upon desodiation. The data gained from simple equivalent circuit fitting shows a lower variation within the SEI and charge transfer resistance for desodiation than for sodiation, explaining the higher apparent diffusion coefficient values during desodiation.
- When conducting PEIS measurements within the plateau region of the HC sodiation/desodiation, a small change in voltage induces a high current response and a large change in sodium concentration. This means that the electrochemical system is not in a semi-equilibrium state. Hence, the interpretation of the calculated values within the plateau region of the HC voltage profile is difficult for EIS-based measurements.

Higher voltage region:

- EIS and EPS are controlled via voltage, leading to higher data resolution. However, as the limitation conditions (current) are met quickly in this voltage region (tens of seconds), a significant double-layer capacitance contribution is observed. The surface capacitance has a time constant proportional to t^{-1} rather than $t^{-0.5}$, leading to errors in

the diffusion estimation.

- The benefit of using a small voltage amplitude during the PEIS measurement to avoid altering the SoC within the plateau region may be too small to cause a reliable, current response. The data gained from the PEIS measurements performed in this study are based on the average value of three iterations per frequency to minimize any errors.
- The pulse length for GITT measurements needs to meet the condition: $\tau \ll \frac{L^2}{D}$l. Nevertheless, due to the steep sloping region, there is the potential to induce a large change in the SoC. This effect is further intensified due to the low electronic conductivity and high overpotentials (IR contributions). Here, the pulse length τ needs to be long enough to induce an actual charge into the material, which is on longer time scales than the ohmic polarization and double-layer forming and capacitance. With sufficient long OCV periods within the GITT measurements, the overpotential can be neglected in discussing the results. In addition, the influence of the sodium metal counter electrode can be neglected when a 3-electrode arrangement is used. Nevertheless, sodium metal is also used as reference material and although there are only measurement currents present, sodium metal is known for surface layer formation within carbonated electrolytes.[35,82]

Differences in the reported diffusion coefficients arise from both experimental set-ups and the assumptions made in the calculations. GITT was developed for a thin film rather than a porous electrode, and therefore the surface area used in the calculation was the electrode area rather than the electrolyte-electrode interface area in a porous electrode. The transport limitation for a thin film is the flux of counter ions to the surface of the film. In a porous electrode, diffusion is assumed to be the flux of ions to the active particles' surface. The effective surface area is difficult to accurately estimate because of the carbon binder domain and embedded particles' in the current collector. It can be estimated from particle size, and in this case, we assume a spherical particle and can use the particle average radii. However, particles are rarely fully spherical, generally have a particle size distribution, and are potentially anisotropic in sodium

ion transport. This results in subtly different true electrochemically active areas. Consequently, this will also affect the accuracy of the calculated diffusion parameters.

5. Conclusions

HC composite electrodes have been studied in a 3-electrode cell set-up to examine the diffusion behaviour of sodium ions using the GITT, EIS, and EPS. All techniques were conducted using the same electrode. Additionally, the importance of the correct cell set-up, as well as parameter settings and analysis, have been discussed, including the relative advantages and limitations.

The collective finding from all techniques conducted indicates a reversible sodiation/desodiation process. Moreover, all generated data shows a dependence of diffusion capability during the SoC for sodiation and desodiation. The same general trend of sodium ion diffusion capability with SoC is derived from each technique showing higher values within the sloping region and lower values within the low voltage plateau. Between these stages, the apparent diffusion coefficient varies by orders of magnitude. Differences in minimum and maximum values are related to parameter settings and quasi-equilibrium state adherence. All test parameters have been optimized to reduce overpotential and probe the transport properties as accurately as possible. Several assumptions are made for analysis, such as spherical particles, and ionic transport, which obeys Fick's law of diffusion in the solid. These may not hold true for materials, which are changing phase or where precipitation is occurring. The combination of these three techniques illustrates three distinct charge storage mechanisms for sodiation in hard carbon, with a combination of these mechanisms being observed in between the different stages.

1. High voltage (>1.3 V vs Na/Na+): sodium ion absorbance at the electrodes' surface is related to a surface capacitance and redox.

2. Intercalation (1.3 – 0.1 V vs Na/Na+) and a solid solution phase associated with sodium ion transport between the graphene sheets, with a higher apparent diffusion coefficient.

3. Two phase low voltage plateau (<0.1V vs Na/Na+) relating to sodium plating in the pores of the carbon structure, which has an extremely low apparent diffusion coefficient.

GITT provides high-resolution information over the whole SoC due to the short current pulses used. This has greater accuracy in the sloping potential regions but disadvantages in the flat potential regions due to dV/dt being close to zero, resulting in very low calculated apparent diffusion coefficients. In addition, generally, a flat voltage indicates a phase change rather than a solid solution. Therefore the description of ionic transport using Ficks Law for all techniques may need reassessing. EIS also exhibits good resolution within the sloping profile range, but inaccuracies can appear when a too high voltage amplitude is used. This is amplified in voltage plateau regions, where the small perturbation may affect a significant sodium concentration change. Further, the EIS data for low potentials also lacks a Warburg feature, likely due to overlapping transport frequencies and mechanisms. EPS has the highest accuracy in regions of steep voltage profiles but has limited accuracy for diffusion coefficient calculations with no voltage change. This is because a small change in voltage can have a significant change in concentration of sodium, such that $t \ll L^2 D^{-1}$ does not hold true. In the case where $t \gg L^2 D^{-1}$ the diffusion can still be calculated; however, there are limited data points. But with optimised and reduced overpotentials, this technique exhibits high accuracy and resolution even in shallow voltage change regions. Each approach has different implications for practical implementation, and there are trade-offs to be considered. Based on the ratio of data points per testing time, GITT and EPS are the techniques of choice. Systematic errors are easier spotted with a higher registration rate per testing time, and the data seems more reliable. Nonetheless, the EIS measurement itself brings much more information if analyzed in full. This work concentrates on diffusion only, and further work is required to probe the kinetics, particularly the specifics of the rate constants for transport at the lower voltage where phase changes occur. It is evident that the shape of the diffusion coefficients gained via GITT and EPS look very similar. EIS has the advantage of being easily implemented into standard test plans and is not as time-consuming as GITT or EPS when used at a single voltage, but is not effective over the

entire SoC range. Hence, these methods are not contradictory but complementary, and a combination of their use is recommended to gain a better overall picture of diffusion characteristics.

Acknowledgements

The authors acknowledge the Royal Commission for the Exhibition of 1851 for the Industrial Fellowship awarded to DL (2015). DB, EK, and PS acknowledge support from the Faraday Institution [grant number FIRG015] and PRS the Royal Academy of Engineering.

References

[1] G.E. Blomgren, The Development and Future of Lithium Ion Batteries, J. Electrochem. Soc. 164 (2016) A5019. https://doi.org/10.1149/2.0251701JES.

[2] M.S. Whittingham, Ultimate Limits to Intercalation Reactions for Lithium Batteries, Chem. Rev. 114 (2014) 11414–11433. https://doi.org/10.1021/cr500049y.

[3] N.I. Zheludev, Y.S. Kivshar, From metamaterials to metadevices, Nat. Mater. 11 (2012) 917–924. https://doi.org/10.1038/nmat3431.

[4] S. Roberts, E. Kendrick, The re-emergence of sodium ion batteries: testing, processing, and manufacturability, Nanotechnol. Sci. Appl. Volume 11 (2018) 23–33. https://doi.org/10.2147/NSA.S146365.

[5] M.J. Lain, E. Kendrick, Understanding the limitations of lithium ion batteries at high rates, J. Power Sources. 493 (2021) 229690. https://doi.org/10.1016/j.jpowsour.2021.229690.

[6] E. Irisarri, A. Ponrouch, M.R. Palacín, M.R. Palacin, Review—Hard Carbon Negative Electrode Materials for Sodium-Ion Batteries, J. Electrochem. Soc. 162 (2015) A2476–A2482. https://doi.org/10.1149/2.0091514jes.

[7] C. Bommier, W. Luo, W.Y. Gao, A. Greaney, S. Ma, X. Ji, Predicting capacity of hard carbon anodes in sodium-ion batteries using porosity measurements, Carbon N. Y. 76 (2014) 165–174. https://doi.org/10.1016/j.carbon.2014.04.064.

[8] J.K. Kirui, J.A. van Wyk, M.J.R. Hoch, ESR studies of the negative divacancy in

irradiated type-I diamonds, Diam. Relat. Mater. 8 (1999) 1569–1571. https://doi.org/10.1016/j.jpowsour.2006.09.001.

[9] K. Smith, J. Treacher, D. Ledwoch, P. Adamson, E. Kendrick, Novel High Energy Density Sodium Layered Oxide Cathode Materials: from Material to Cells, ECS Trans. 75 (2017) 13–24. https://doi.org/10.1149/07522.0013ecst.

[10] H.O. Pierson, Handbook of Carbon, Graphite, Diamond and Fullerenes, First, Noyes Publications, 1993. https://doi.org/http://dx.doi.org/10.1016/B978-0-8155-1339-1.50008-6.

[11] D.A. Stevens, J.R. Dahn, High Capacity Anode Materials for Rechargeable Sodium-Ion Batteries, J. Electrochem. Soc. 147 (2000) 1271. https://doi.org/10.1149/1.1393348.

[12] C. Bommier, T.W. Surta, M. Dolgos, X. Ji, New Mechanistic Insights on Na-Ion Storage in Nongraphitizable Carbon, Nano Lett. 15 (2015) 5888–5892. https://doi.org/10.1021/acs.nanolett.5b01969.

[13] P. Thomas, D. Billaud, Effect of mechanical grinding of pitch-based carbon fibers and graphite on their electrochemical sodium insertion properties, Electrochim. Acta. 46 (2000) 39–47. https://doi.org/10.1016/S0013-4686(00)00542-9.

[14] C.M. Wu, P.I. Pan, Y.W. Cheng, C.P. Liu, C.C. Chang, M. Avdeev, S. kang Lin, The mechanism of the sodiation and desodiation in Super P carbon electrode for sodium-ion battery, J. Power Sources. 340 (2017) 14–21. https://doi.org/10.1016/j.jpowsour.2016.11.048.

[15] S. Alvin, D. Yoon, C. Chandra, H.S. Cahyadi, J.H. Park, W. Chang, K.Y. Chung, J. Kim, Revealing sodium ion storage mechanism in hard carbon, Carbon N. Y. 145 (2019) 67–81. https://doi.org/10.1016/j.carbon.2018.12.112.

[16] J.M. Stratford, P.K. Allan, O. Pecher, P.A. Chater, C.P. Grey, Mechanistic insights into sodium storage in hard carbon anodes using local structure probes, Chem. Commun. 52 (2016) 12430–12433. https://doi.org/10.1039/C6CC06990H.

[17] S. Komaba, W. Murata, T. Ishikawa, N. Yabuuchi, T. Ozeki, T. Nakayama, A. Ogata, K. Gotoh, K. Fujiwara, Electrochemical Na insertion and solid electrolyte interphase for hard-carbon electrodes and application to Na-ion batteries, Adv. Funct. Mater. 21 (2011)

3859–3867. https://doi.org/10.1002/adfm.201100854.

[18] X. Li, X. Zeng, T. Ren, J. Zhao, Z. Zhu, S. Sun, Y. Zhang, The transport properties of sodium-ion in the low potential platform region of oatmeal-derived hard carbon for sodium-ion batteries, J. Alloys Compd. 787 (2019) 229–238. https://doi.org/10.1016/j.jallcom.2019.02.077.

[19] Q. Wang, X. Zhu, Y. Liu, Y. Fang, X. Zhou, J. Bao, Rice husk-derived hard carbons as high-performance anode materials for sodium-ion batteries, Carbon N. Y. 127 (2018) 658–666. https://doi.org/10.1016/j.carbon.2017.11.054.

[20] J.S. Weaving, A. Lim, J. Millichamp, T.P. Neville, D. Ledwoch, E. Kendrick, P.F. McMillan, P.R. Shearing, C.A. Howard, D.J.L. Brett, Elucidating the sodiation mechanism in hard carbon by operando raman spectroscopy, ACS Appl. Energy Mater. 3 (2020) 7474–7484. https://doi.org/10.1021/acsaem.0c00867.

[21] C.-H. Chen, F. Brosa Planella, K. O'Regan, D. Gastol, W.D. Widanage, E. Kendrick, Development of Experimental Techniques for Parameterization of Multi-scale Lithium-ion Battery Models, J. Electrochem. Soc. 167 (2020) 080534. https://doi.org/10.1149/1945-7111/ab9050.

[22] M. Okoshi, Y. Yamada, A. Yamada, H. Nakai, Theoretical Analysis on De-Solvation of Lithium, Sodium, and Magnesium Cations to Organic Electrolyte Solvents, J. Electrochem. Soc. 160 (2013) A2160–A2165. https://doi.org/10.1149/2.074311jes.

[23] A. Ponrouch, D. Monti, A. Boschin, B. Steen, P. Johansson, M.R. Palacín, Non-aqueous electrolytes for sodium-ion batteries, J. Mater. Chem. A. 3 (2015) 22–42. https://doi.org/10.1039/c4ta04428b.

[24] E. Jónsson, P. Johansson, Modern battery electrolytes: Ion-ion interactions in Li+/Na+conductors from DFT calculations, Phys. Chem. Chem. Phys. 14 (2012) 10774–10779. https://doi.org/10.1039/c2cp40612h.

[25] F. Sagane, T. Abe, Z. Ogumi, Sodium-ion transfer at the interface between ceramic and organic electrolytes, J. Power Sources. 195 (2010) 7466–7470. https://doi.org/10.1016/j.jpowsour.2010.04.054.

[26] Y. Mizuno, M. Okubo, D. Asakura, T. Saito, E. Hosono, Y. Saito, K. Oh-Ishi, T. Kudo,

H. Zhou, Impedance spectroscopic study on interfacial ion transfers in cyanide-bridged coordination polymer electrode with organic electrolyte, Electrochim. Acta. 63 (2012) 139–145. https://doi.org/10.1016/j.electacta.2011.12.068.

[27] R. Ramachandran, S.M. Chen, G.P. Gnana Kumar, Recent developments in electrode materials for oxygen reduction reaction, Int. J. Electrochem. Sci. 10 (2015) 8581–8606. https://doi.org/10.1039/C4TA06467D.

[28] A.H. Thompson, Electrochemical Potential Spectroscopy: A New Electrochemical Measurement, J. Electrochem. Soc. 126 (1979) 608. https://doi.org/10.1149/1.2129095.

[29] J. Barker, R. Pynenburg, R. Koksbang, Determination of thermodynamic, kinetic and interfacial properties for the Li//LixMn2O4 system by electrochemical techniques, J. Power Sources. 52 (1994) 185–192. https://doi.org/10.1016/0378-7753(94)01958-4.

[30] W. Weppner, R.A. Huggins, Determination of the Kinetic Parameters of Mixed-Conducting Electrodes and Application to the System Li3Sb, J. Electrochem. Soc. 124 (1977) 1569–1578.

[31] W. Luo, C. Bommier, Z. Jian, X. Li, R. Carter, S. Vail, Y. Lu, J.J. Lee, X. Ji, Low-surface-area hard carbon anode for Na-ion batteries via graphene oxide as a dehydration agent, ACS Appl. Mater. Interfaces. 7 (2015) 2626–2631. https://doi.org/10.1021/am507679x.

[32] Y. Li, Y.S. Hu, M.M. Titirici, L. Chen, X. Huang, Hard Carbon Microtubes Made from Renewable Cotton as High-Performance Anode Material for Sodium-Ion Batteries, Adv. Energy Mater. 6 (2016). https://doi.org/10.1002/aenm.201600659.

[33] K. Wang, Y. Jin, S. Sun, Y. Huang, J. Peng, J. Luo, Q. Zhang, Y. Qiu, C. Fang, J. Han, Low-Cost and High-Performance Hard Carbon Anode Materials for Sodium-Ion Batteries, ACS Omega. 2 (2017) 1687–1695. https://doi.org/10.1021/acsomega.7b00259.

[34] D. Ledwoch, J.B. Robinson, D. Gastol, K. Smith, P.R. Shearing, D.J.L. Brett, E. Kendrick, Hard Carbon Composite Electrodes for Sodium-Ion Batteries with Nano-Zeolite and Carbon Black Additives, Batter. Supercaps. 4 (2021) 163–172. https://doi.org/10.1002/batt.202000161.

[35] D. Ledwoch, E. Kendrick, P. Adamson, Composite Electrode including microporous

ionically conducting material, composite slurry, and methods of manufacturing same (Application), US20180287134 A1, 2017.

[36] W. Weppner, R.A. Huggins, Electrochemical Methods for Determining Kinetic Properties of Solids, Annu. Rev. Mater. Sci. 8 (1978) 269–311. https://doi.org/10.1146/annurev.ms.08.080178.001413.

[37] M.D. Levi, D. Aurbach, Diffusion Coefficients of Lithium Ions during Intercalation into Graphite Derived from the Simultaneous Measurements and Modeling of Electrochemical Impedance and Potentiostatic Intermittent Titration Characteristics of Thin Graphite Electrodes, J. Phys. Chem. B. 101 (1997) 4641–4647. https://doi.org/10.1021/jp9701911.

[38] D. Ledwoch, D.J.L. Brett, E. Kendrick, The Performance of Hard Carbon in a Sodium Ion Battery and Influence of the Sodium Metal in Observed Properties, ECS Trans. 72 (2016) 17–22. https://doi.org/10.1149/07233.0017ecst.

[39] D. Ledwoch, D.J.L.L. Brett, P.R. Shearing, E. Kendrick, Investigation of the Sodiation and Desodiation of Hard Carbon by Electrochemical Testing and X-Ray Computed Tomography, ECS Trans. 75 (2017) 81–90. https://doi.org/10.1149/07552.0081ecst.

[40] F. La Mantia, C.D. Wessells, H.D. Deshazer, Y. Cui, Reliable reference electrodes for lithium-ion batteries, Electrochem. Commun. 31 (2013) 141–144. https://doi.org/10.1016/j.elecom.2013.03.015.

[41] J.R. Belt, D.M. Bernardi, V. Utgikar, Development and Use of a Lithium-Metal Reference Electrode in Aging Studies of Lithium-Ion Batteries, J. Electrochem. Soc. 161 (2014) A1116–A1126. https://doi.org/10.1149/2.062406jes.

[42] D.P. Abraham, S.D. Poppen, A.N. Jansen, J. Liu, D.W. Dees, Application of a lithium-tin reference electrode to determine electrode contributions to impedance rise in high-power lithium-ion cells, Electrochim. Acta. 49 (2004) 4763–4775. https://doi.org/10.1016/j.electacta.2004.05.040.

[43] S. Klink, E. Madej, E. Ventosa, A. Lindner, W. Schuhmann, F. La Mantia, The importance of cell geometry for electrochemical impedance spectroscopy in three-electrode lithium ion battery test cells, Electrochem. Commun. 22 (2012) 120–123.

https://doi.org/10.1016/j.elecom.2012.06.010.

[44] C.J. Wen, B.A. Boukamp, R.A. Huggins, Thermodynamic and Mass Transport Properties of "LiAl," J. Electrochem. Soc. 126 (1979) 2258–2266.

[45] D.W. Dees, S. Kawauchi, D.P. Abraham, J. Prakash, Analysis of the Galvanostatic Intermittent Titration Technique (GITT) as applied to a lithium-ion porous electrode, J. Power Sources. 189 (2009) 263–268. https://doi.org/10.1016/j.jpowsour.2008.09.045.

[46] W. Weppner, R.A. Huggins, Electrochemical investigation of the chemical diffusion, partial ionic conductivities, and other kinetic parameters in Li3Sb and Li3Bi, J. Solid State Chem. 22 (1977) 297–308. https://doi.org/10.1016/0022-4596(77)90006-8.

[47] M. V. Reddy, R. Jose, A. Le Viet, K.I. Ozoemena, B.V.R. Chowdari, S. Ramakrishna, Studies on the lithium ion diffusion coefficients of electrospun Nb 2O5 nanostructures using galvanostatic intermittent titration and electrochemical impedance spectroscopy, Electrochim. Acta. 128 (2014) 198–202. https://doi.org/10.1016/j.electacta.2013.10.003.

[48] S. Alvin, H.S. Cahyadi, J. Hwang, W. Chang, S.K. Kwak, J. Kim, Revealing the Intercalation Mechanisms of Lithium, Sodium, and Potassium in Hard Carbon, Adv. Energy Mater. 10 (2020) 2000283. https://doi.org/10.1002/aenm.202000283.

[49] Y. Zhu, C. Wang, Galvanostatic intermittent titration technique for phase-transformation electrodes, J. Phys. Chem. C. 114 (2010) 2830–2841. https://doi.org/10.1021/jp9113333.

[50] J. Barker, D. Baldwin, D.C. Bott, S.J. Porter, Electrochemical voltage spectroscopy; Dopant diffusion in Durham polyacetylene, Synth. Met. 28 (1989). https://doi.org/10.1016/0379-6779(89)90682-6.

[51] J. Barker, Three Electrode Electrochemical Voltage Spectroscopy (TEVS): evaluation of a model lithium ion system, Electrochim. Acta. 40 (1995) 1603–1608. https://doi.org/10.1016/0013-4686(95)00090-2.

[52] J. Barker, R. Pynenburg, R. Koksbang, M.Y. Saidi, An electrochemical investigation into the lithium insertion properties of LixCoO2, Electrochim. Acta. 41 (1996) 2481–2488. https://doi.org/10.1016/0013-4686(96)00036-9.

[53] A.J. Bard, L.R. Faulkner, Electrochemical Methods, Second, John Wiley & Sons, 2001.

[54] R. Li, J. Huang, Z. Xu, H. Qi, L. Cao, Y. Liu, W. Li, J. Li, Controlling the Thickness of

Disordered Turbostratic Nanodomains in Hard Carbon with Enhanced Sodium Storage Performance, Energy Technol. 6 (2018) 1080–1087. https://doi.org/10.1002/ente.201700674.

[55] E. Barsoukov, Kinetics of lithium intercalation into carbon anodes: in situ impedance investigation of thickness and potential dependence, Solid State Ionics. 116 (1999) 249–261. https://doi.org/10.1016/j.visres.2004.04.013.

[56] C.J. Wen, Chemical Diffusion in Lithium Alloys, Stanford University, 1980.

[57] Q. Zhuang, X. Qiu, S.-D. Xu, Y.-H. Qiang, S.-G. Su, S.-G. Sun, Diagnosis of Electrochemical Impedance Spectroscopy in Lithium-Ion Batteries, in: I. Belharouak (Ed.), Lithium Ion Batter. - New Dev., InTech, 2012: pp. 189–226. https://doi.org/10.5772/26749.

[58] L. Wang, J. Zhao, X. He, J. Gao, J. Li, C. Wan, C. Jiang, Electrochemical Impedance Spectroscopy (EIS) study of LiNi1/3Co1/3Mn1/3O2for Li-ion batteries, Int. J. Electrochem. Sci. 7 (2012) 345–353.

[59] M.D. Levi, G. Salitra, B. Markovsky, H. Teller, D. Aurbach, U. Heider, L. Heider, Solid-State Electrochemical Kinetics of Li-Ion Intercalation into Li 1-x CoO 2 : Simultaneous Application of Electroanalytical Techniques SSCV, PITT, and EIS, J. Electrochem. Soc. 146 (1999) 1279. https://doi.org/10.1149/1.1391759.

[60] H. Liu, C. Li, H.P. Zhang, L.J. Fu, Y.P. Wu, H.Q. Wu, Kinetic study on LiFePO4/C nanocomposites synthesized by solid state technique, J. Power Sources. 159 (2006) 717–720. https://doi.org/10.1016/j.jpowsour.2005.10.098.

[61] S. Liu, S. Tang, X. Zhang, A. Wang, Q.H. Yang, J. Luo, Porous Al Current Collector for Dendrite-Free Na Metal Anodes, Nano Lett. 17 (2017) 5862–5868. https://doi.org/10.1021/acs.nanolett.7b03185.

[62] F. Linsenmann, D. Pritzl, H.A. Gasteiger, A Reference Electrode for In Situ Impedance Measurements in Sodium-Ion Batteries, J. Electrochem. Soc. 166 (2019) A3668–A3674. https://doi.org/10.1149/2.0741915jes.

[63] J. Landesfeind, D. Pritzl, H.A. Gasteiger, An Analysis Protocol for Three-Electrode Li-Ion Battery Impedance Spectra: Part I. Analysis of a High-Voltage Positive Electrode, J.

Electrochem. Soc. 164 (2017) A1773–A1783. https://doi.org/10.1149/2.0131709jes.

[64] Bio-Logics Science Instruments, How to interpret lower frequencies impedance in batteries?, EC-Lab – Appl. Note #61. (2017).

[65] V. Simone, A. Boulineau, A. de Geyer, D. Rouchon, L. Simonin, S. Martinet, Hard carbon derived from cellulose as anode for sodium ion batteries: Dependence of electrochemical properties on structure, J. Energy Chem. 25 (2016) 761–768. https://doi.org/10.1016/j.jechem.2016.04.016.

[66] R. Väli, A. Jänes, T. Thomberg, E. Lust, D-Glucose Derived Nanospheric Hard Carbon Electrodes for Room-Temperature Sodium-Ion Batteries, J. Electrochem. Soc. 163 (2016) A1619–A1626. https://doi.org/10.1149/2.0771608jes.

[67] J.M. Bray, C.L. Doswell, G.E. Pavlovskaya, L. Chen, B. Kishore, H. Au, H. Alptekin, E. Kendrick, M.M. Titirici, T. Meersmann, M.M. Britton, Operando visualisation of battery chemistry in a sodium-ion battery by 23Na magnetic resonance imaging, Nat. Commun. 11 (2020) 1–10. https://doi.org/10.1038/s41467-020-15938-x.

[68] J.P. Meyers, M. Doyle, R.M. Darling, J. Newman, The Impedance Response of a Porous Electrode Composed of Intercalation Particles, J. Electrochem. Soc. 147 (2000) 2930. https://doi.org/10.1149/1.1393627.

[69] E. Barsoukov, J.R. Macdonald, Impedance Spectroscopy, Second, John Wiley & Sons, 2011. https://doi.org/10.1037//0735-7028.32.2.142.

[70] E.-M.M. Hammer, B. Berger, L. Komsiyska, Improvement of the Performance of Graphite Felt Electrodes for Vanadium-Redox-Flow-Batteries by Plasma Treatment, Int. J. Renew. Energy Dev. 3 (2014) 7–12. https://doi.org/10.14710/ijred.3.1.7-12.

[71] C. Wang, A.J. Appleby, F.E. Little, Electrochemical impedance study of initial lithium ion intercalation into graphite powders, Electrochim. Acta. 46 (2001) 1793–1813. https://doi.org/10.1016/S0013-4686(00)00782-9.

[72] S.H. Yu, C.K. Park, H. Jang, C.B. Shin, W. Il Cho, Prediction of lithium diffusion coefficient and rate performance by using the discharge curves of LiFePO4 materials, Bull. Korean Chem. Soc. 32 (2011) 852–856. https://doi.org/10.5012/bkcs.2011.32.3.852.

[73] C.K. Park, S. Bin Park, S.H. Oh, H. Jang, W. Il Cho, Li ion diffusivity and improved electrochemical performances of the carbon coated LiFePO4, Bull. Korean Chem. Soc. 32 (2011) 836–840. https://doi.org/10.5012/bkcs.2011.32.3.836.

[74] P. Yu, B.N. Popov, J.A. Ritter, R.E. White, Z.Y. Tang, J.J. Xue, C.Y. Liu, X.G. Zhuang, Determination of the Lithium Ion Diffusion Coefficient in Graphite Anode Material, Acta Phys. - Chim. Sin. 17 (2001) 388. https://doi.org/10.1149/1.1391556.

[75] C. Bommier, D. Leonard, Z. Jian, W.F. Stickle, P.A. Greaney, X. Ji, New Paradigms on the Nature of Solid Electrolyte Interphase Formation and Capacity Fading of Hard Carbon Anodes in Na-Ion Batteries, Adv. Mater. Interfaces. 3 (2016) 1600449. https://doi.org/10.1002/admi.201600449.

[76] L. Chen, B. Kishore, M. Walker, C.E.J. Dancer, E. Kendrick, Nanozeolite ZSM-5 electrolyte additive for long life sodium-ion batteries, Chem. Commun. (2020). https://doi.org/10.1039/D0CC03976D.

[77] H. Au, H. Alptekin, A.C.S. Jensen, E. Olsson, C.A. O'Keefe, T. Smith, M. Crespo-Ribadeneyra, T.F. Headen, C.P. Grey, Q. Cai, A.J. Drew, M.-M. Titirici, A revised mechanistic model for sodium insertion in hard carbons, Energy Environ. Sci. 13 (2020) 3469–3479. https://doi.org/10.1039/D0EE01363C.

[78] H.Y. Yu, H.J. Liang, Z.Y. Gu, Y.F. Meng, M. Yang, M.X. Yu, C. De Zhao, X.L. Wu, Waste-to-wealth: low-cost hard carbon anode derived from unburned charcoal with high capacity and long cycle life for sodium-ion/lithium-ion batteries, Electrochim. Acta. 361 (2020) 137041. https://doi.org/10.1016/J.ELECTACTA.2020.137041.

[79] K. Gotoh, T. Ishikawa, S. Shimadzu, N. Yabuuchi, S. Komaba, K. Takeda, A. Goto, K. Deguchi, S. Ohki, K. Hashi, T. Shimizu, H. Ishida, NMR study for electrochemically inserted Na in hard carbon electrode of sodium ion battery, J. Power Sources. 225 (2013) 137–140. https://doi.org/10.1016/j.jpowsour.2012.10.025.

[80] M. Meyer, L. Komsiyska, B. Lenz, C. Agert, Study of the local SOC distribution in a lithium-ion battery by physical and electrochemical modeling and simulation, Appl. Math. Model. 37 (2013) 2016–2027. https://doi.org/10.1016/j.apm.2012.04.029.

[81] Z. Liu, Y.Y. Hu, M.T. Dunstan, H. Huo, X. Hao, H. Zou, G. Zhong, Y. Yang, C.P. Grey,

Local structure and dynamics in the Na ion battery positive electrode material Na3V2(PO4)2F3, Chem. Mater. 26 (2014) 2513–2521. https://doi.org/10.1021/cm403728w.

[82] L. Gao, J. Chen, Y. Liu, Y. Yamauchi, Z. Huang, X. Kong, Revealing the chemistry of an anode-passivating electrolyte salt for high rate and stable sodium metal batteries, J. Mater. Chem. A. 6 (2018) 12012–12017. https://doi.org/10.1039/c8ta03436b.